Chemical Engineering Science 71 (2012) 300–309

Contents lists available at SciVerse ScienceDirect

Chemical Engineering Science

journal homepage: www.elsevier.com/locate/ces

Analysis of flow through an orifice meter: CFD simulation

Manish S. Shah [a,c], Jyeshtharaj B. Joshi [1,a,b,*], Avtar S. Kalsi [c], C.S.R. Prasad [c], Daya S. Shukla [c]

[a] Department of Chemical Engineering, Institute of Chemical Technology, Matunga, Mumbai 400019, India
[b] Homi Bhabha National Institute, Trombay, Mumbai 400094, India
[c] Chemical Technology Division, Bhabha Atomic Research Center, Trombay, Mumbai 400085, India

ARTICLE INFO

Article history:
Received 29 July 2011
Received in revised form
11 November 2011
Accepted 14 November 2011
Available online 1 December 2011

Keywords:
Chemical processes
Instrumentation
Simulation
Turbulence
Openfoam
Vena-contracta

ABSTRACT

Orifice meters are the most common instruments used for fluid flow measurement because of its ruggedness, simple mechanical construction and other known advantages. Orifice coefficients are empirical because of difficulty in accurately predicting the effects of geometrical complicacy and flow separation from the wall on the flow. In the present paper, Computational Fluid Dynamics (CFD) simulation has been used to predict the orifice flow with better accuracy. CFD simulations have been performed using OpenFOAM-1.6 solver and validated with the published experimental data of Nail (1991) and Morrison et al. (1993). CFD simulations have been validated with pressure drop and energy balance of our experimental data of water as fluid. The outcomes of the CFD simulations in terms of profiles of velocity, pressure, etc. are discussed in detail. A new scheme has been proposed to track vena-contracta with the help of CFD and with a suitable provision in the hardware of orifice meter. The new scheme maintains the existing advantages of orifice meters and provides better accuracy and sensitivity.

1. Introduction

It is very important to have information on flow rates of various chemical process streams with adequate accuracy in the plants, especially when it has a direct influence on efficiency and productivity of a given process. Although orifice meters have higher pressure losses and correspondingly higher pumping cost, they are still the most common meters used for fluid flow measurement because these are rugged, simple in construction and installation/replacement, without having any moving parts, economic, measurement flexibility with high rangeability, can be used for liquids, gases or slurries, well suited for use under extreme weather conditions, etc. (Husain, 2010 and McCabe et al. 1993). It works on simple principle of using effects of velocity and pressure variation caused by reduction of the available area for flow. Orifice meters are well known and have been studied by a number of investigators over a considerable range of Reynolds numbers and Beta ratio (Nail (1991); Morrison et al. (1993); Smith et al. (2008), Naveenji et al. (2010); Oliveira et al. (2010)). In international trade, it is implemented in accordance with international standards such as ISO 5167-1. The orifice meter is supplied with discharge coefficient (C_D) and installation procedure. The discharge coefficient is defined as the ratio of actual flow to the theoretical flow. It is obtained from experimental measurements after regression, wherein experiments are conducted in controlled conditions of undisturbed, symmetrical, swirl-free velocity profile in the upstream of orifice (Erdal and Andersson (1997)). Definite straight length of pipe is also kept downstream of the orifice to avoid the effects of outlet conditions on the flow profile close to downstream of orifice. With the above distinct advantages of a flow meter of high industrial importance, authors felt necessary to understand the flow pattern of orifice meter to further improve its performance in terms of flow measurement with better accuracy and sensitivity.

2. Previous work

The summary of published literature is given in Table 1. Very few attempts have been made to simulate the flow pattern for orifice with the help of Computational Fluid Dynamics (CFD). Durst and Wang, 1989 found good agreement between calculations using k–ε turbulence model and measurements, but pressure drop was not reported by them. Smith et al. (2008) have studied the effect of beta ratios from 0.5 to 0.8 on the flow field. Naveenji et al. (2010) have studied variation in discharge coefficient for non-Newtonian fluid flow at beta ratios from 0.4 to 0.8. Oliveira et al. (2010) have presented numerical methodology

* Corresponding author at: Institute of Chemical Technology, Department of Chemical Engineering, Matunga, Mumbai, Maharastra 400019, India.
Tel.: +91 22 3361 2106, fax: +91 22 3361 1020.
E-mail address: jbjsohi@gmail.com (J.B. Joshi).
[1] Tel.: +91 22 2559 7625.

0009-2509/$ - see front matter © 2011 Elsevier Ltd. All rights reserved.
doi:10.1016/j.ces.2011.11.022

Table 1
Summary of previous works.

Author	Pipe diameter (mm)	β	Working fluid	Range of *Re*	Remarks
Ho and Leung (1985)	25.4	0.247, 0.36, 0.448	water	100–1000	Low *Re* (laminar flow) experiments. Variation in C_D vs. *Re* presented.
Nail (1991)	25.4	0.5	air	18,400	Experiments using 3 Dimensional LDA technique.
Morrison et al. (1993)	50.8	0.5	air	91,100	Experiments using 3 Dimensional LDA technique. Measured mean velocity and wall pressure. Turbulence quantities calculated and discussed in detail.
Smith et al. (2008)	25.4	0.5, 0.6, 0.8	air	18,400	Effect of turbulence models (k–ε and RSM) on mean axial velocity and wall pressure studied using CFD simulation and compared with experimental data of Nail.
Naveenji et al. (2010)	50, 100, 200	0.4–0.8	Non-Newtonian fluids (prepared with varying concentration of salt)	100–10,000	C_D vs. *Re* predicted using CFD simulation.
Oliveira et al. (2010)	100	0.1–0.6	water	4000–10^6	Predicted pressure drop vs. flow rate with various values of β, C_D vs. *Re* and wall pressure using CFD simulation.

for calibrating orifice meter. CFD technique requires reliable experimental data on flow profiles to validate its outcome. In all the above literature, limited part of CFD simulations have been compared with experimental data. Nail (1991) has presented experimental measurements of centerline axial velocities, wall-static pressure, Renoylds' stresses and wall shear stresses measured using Laser Doppler Anemometer (LDA) in his PhD Dissertation. Morrison et al. (1993) have measured flow field using a three-color, 3D LDA and reported the mean velocity and turbulence field inside orifice flow meter with a beta ratio of 0.5. Centerline axial velocity and wall pressure profiles were also presented. To summarise, though reliable experimental data are available, comprehensive information is not available in the published literature on the predicted flow structure downstream of orifice explaining the flow features using CFD simulations. Moreover, advancement in the CFD, availability of high speed computing machines and robust solvers have encouraged us to make an attempt for predicting orifice flows with better accuracy. It was also thought desirable to propose a cost effective tool towards replacement of experiments required for estimating the discharge coefficient. In the present paper, efforts are made to combine experimental and CFD modeling to achieve better explanation for the flow phenomena in the upstream and downstream of orifice. Experiments are conducted with water as fluid with various flow rates. Pressure drop across the orifice meter was measured with the help of manometer mounted on flange taps of the meter. CFD simulations have been carried out and compared with experimental data using water (up to 3 ms^{-1} pipe velocity) and published experimental data of Nail (1991) and Morrison et al. (1993). Energy balance is also established for the simulated cases. Sensitivity analysis of turbulence model parameters has also been reported in the present work. Typical geometry of orifice meter considered for all the simulations is given in Fig. 1.

It is also known that the actual locations of vena-contracta change with flow rates and may not match the vena-contracta tapping. It is shown that in the CFD simulation, it is possible to locate the vena-contracta. Using this capability of CFD, a suitable modification in the hardware has been proposed to position the pressure tap at vena-contracta for flow measurement with better accuracy and sensitivity without compromising the existing advantages of orifice meter.

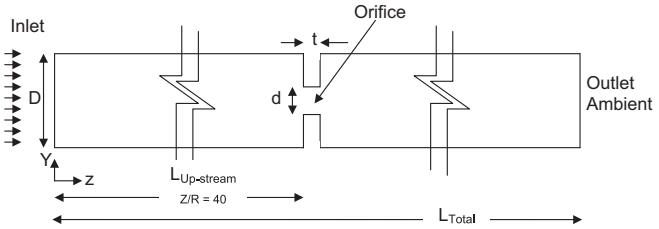

Fig. 1. Typical orifice geometry considered for simulation (orifice is at z/R=40 from inlet).

3. Numerical procedure

3.1. Governing equations

In order to simulate the steady state flow through an orifice meter, the governing equations (continuity and momentum) with the appropriate Reynolds stress closure need to be solved. In the present work, standard k–ε turbulence model by Launder and Spalding (1972) has been used. The k–ε turbulence model is simple to use, most widely validated and has excellent performance for many industrially relevant flows (Versteeg and Malalasekera (1995); Thakre and Joshi (2002)). It also requires less computational power compared to more general Reynolds Stress Model. All the governing equations are given in Table 2.

3.2. Grid independence

A grid independence study was performed to find the mesh size that was sufficiently fine so that solution does not change by further refining the mesh. The velocity profiles and pressure profiles for 351,360 hexahedral cells and 10,47,360 hexahedral cells are given in Fig. 2. No appreciable change has been found in velocity and pressure profiles for coarse and fine meshes. However, there has been improvement in the energy balance with an error reduction of predicted pressure drop from 13.34% to 5.59%.

3D simulations have been carried out for water and air with different values of β, inlet velocity and pipe diameter. The geometrical parameters and grid details are given in Table 3. Adequate length at the upstream and downstream of the orifice plate is provided to avoid the effect of patched boundary

Table 2
Governing equations for steady incompressible flow.

Property	Equations	Boundary condition
Continuity	$\nabla\cdot(\rho\langle u_k\rangle)=0$	At the inlet, inlet velocity is set and pressure gradient is set as zero $(\frac{\partial p}{\partial z}=0)$. At the outlet, outlet ambient pressure is set and velocity gradient is set as zero. At Wall, no slip condition is set.
Momentum	$\nabla\cdot(\rho\langle u_k\rangle\langle u_k\rangle)=-\nabla\langle p\rangle+\nabla\cdot\overline{\tau}_k+\rho\vec{g}$	
	$\overline{\tau}_k=\mu_{eff}\left(\nabla\langle u_k\rangle+(\nabla\langle u_k\rangle)^T-\frac{2}{3}\mu_{eff}\nabla\bullet\langle u_k\rangle I\right)$	
Turbulent kinetic energy	$\nabla\cdot((\langle u_k\rangle\rho k))=\nabla\cdot\left[\left(\mu+\frac{\mu_t}{\sigma_k}\right)\nabla\cdot k\right]+G_k$	
Energy dissipation rate equation	$\frac{\partial(\rho\varepsilon\langle u_k\rangle)}{\partial x_k}=\frac{\partial}{\partial x_k}\left(\left(\mu+\frac{\mu_T}{\sigma_\varepsilon}\right)\frac{\partial\varepsilon}{\partial x_k}\right)+C_{\varepsilon1}\frac{\varepsilon}{k}G_k-C_{\varepsilon2}\frac{\varepsilon^2}{k}$	
	$G_k=\tau_{ik}\frac{\partial\langle u_i\rangle}{\partial x_k}\quad v_T=C_\mu\frac{k^2}{\varepsilon}$	
	$C_\mu=0.09;\sigma_k=1.00;\sigma_\varepsilon=1.3;C_{\varepsilon1}=1.44;C_{\varepsilon2}=1.92$	

Under relaxation parameters: pressure=0.3; momentum=0.7; turbulent kinetic energy=0.8; turbulent energy dissipation rate=0.8.

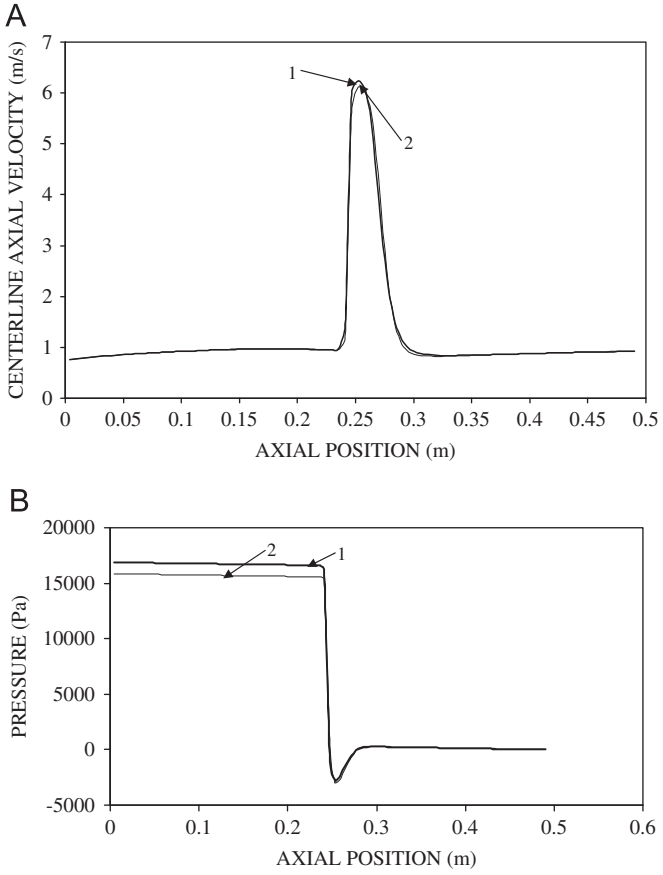

Fig. 2. Effect of grid size on (A) centerline axial velocity and (B) centerline pressure profile with (1) 321,360 cells, (2) with 10,47,360 cells.

conditions on the flow through orifice and ensure fully developed turbulent flow in the upstream of the orifice plate. It was ensured that at least one grid be in the viscous sublayer ($y^+<5$) and several nodes in the buffer and turbulent zones for fine meshes in the orifice region.

Unstructured hexahedral meshes have been used in all the simulations. Typical mesh of a small section of 12.3 mm pipe diameter is shown in Fig. 3. This ensures minimum numerical diffusion. Good quality mesh has been ensured with skewness and aspect ratio at an optimum value. Gradients of pressure and velocity fields are discretized with second order Gaussian finite volume integration using linear interpolation. Gaussian finite volume integration is most common and is based on summing values on cell faces, which must be interpolated from cell to cell. Diversion terms are discretized with first order bounded Gaussian finite volume integration using upwind scheme for interpolation. The selected schemes ensure stable solution. This combination was also found very robust by Erdal and Andersson (1997) for orifice flow simulation. In all the simulations, pre-conditioned bi-conjugate gradient (Vander Vorst, 1981) type solvers are chosen for all the variables except for the pressure for which pre-conditioned conjugate gradient type solver is selected.

3.3. Boundary conditions

In all the simulations, velocity is set at the inlet of the orifice meter, pressure is set at the outlet and no-slip condition is set at the wall. The standard $k-\varepsilon$ model has been used as a turbulence model. The following additional boundary conditions have been used:

I_T=Turbulent intensity=5% can be reasonably assumed at the inlet for fully developed turbulent flow (Thakre and Joshi (2000, 2002)):

$$I_T=\left(\frac{\sqrt{k}}{v_{avg}}\right) \tag{1}$$

$$k=I_T^2u_{avg}^2 \tag{2}$$

So the inlet boundary condition for the turbulent kinetic energy is specified using Eq. (2) Turbulent dissipation energy is given as

$$\varepsilon=C_\mu^{3/2}\frac{k^{3/2}}{l} \tag{3}$$

$$l=(0.09)^{3/4}\frac{k^{3/2}}{\varepsilon}=0.16\frac{k^{3/2}}{\varepsilon} \tag{4}$$

By rearranging

$$\varepsilon\cong\frac{k^{3/2}}{6l} \tag{5}$$

where l is 1/20 to 1/10 of D in pipe. By selecting the first value, we get

$$\varepsilon=\frac{k^{3/2}}{6((1/20)D)} \tag{6}$$

which gives

$$\varepsilon=\frac{k^{3/2}}{0.3D} \tag{7}$$

So the inlet boundary condition for the turbulent energy dissipation is specified using Eq. (7). Boundary conditions are given in Table 4.

Table 3
Geometrical and mesh details of CFD simulations.

Case no.	fluid	Orifice dimensions					Remarks
		Pipe diameter (mm)	β	L_U (mm)	L_T (mm)	t (mm)	
1	Water	12.3	0.4065	246	494	2	Experiments are conducted in the present study. Coarse mesh—321,360 cells Fine mesh—10,47,360 cells
2	Water	12.3	0.162	246	494	2	Mesh used—49,695 hexahedra cells
3	Water	12.3	0.081	246	494	2	Mesh used—12,13,950 hexahedra cells
4	Air	25.4	0.5	500	1200	3.75	Experimental data of Morrison et al. (1993) used for comparison Mesh used—283,700 hexahedra cells
5	Air	50.8	0.5	50.8	228.6	3.2	Experimental data of Nail (1991) used for comparison Mesh used—112,700 hexahedra cells

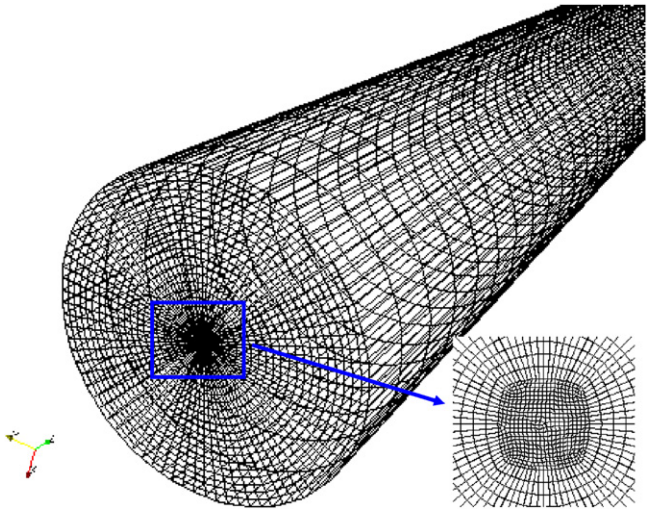

Fig. 3. Typical unstructured hexahedral mesh for 12.3 mm pipe diameter.

Table 4
Boundary conditions for various CFD simulations.

Case no.	Fluid	Sr. No.	Velocity (m/s) inlet	Turbulent kinetic energy (m^2/s^2) inlet	Turbulent dissipation rate (m^2/s^3) inlet	Turbulent viscosity (m^2/s) inlet
1	Water	1	0.376	0.00053	0.00002	0.001264
		2	0.482	0.00087	0.00004	0.001703
		3	0.673	0.0017	0.00014	0.0021675
		4	0.755	0.00214	0.00016	0.002944
		5	1	0.00375	0.01534	0.00825
		6	2	0.015	0.1227	0.00165
		7	3	0.03375	0.41415	0.00248
2	Water	8	0.755	0.00214	0.00661	0.002944
3	Water	9	0.755	0.00214	0.00661	0.002944
4	Air	10	28.087	2.958	5.573	0.1413
5	Air	11	11.344	0.004826	0.01084	0.000193

3.4. Solution procedure

The governing equations have been solved for steady state conditions using the open source CFD code OpenFOAM-1.6 with simpleFoam solver. All the discretized equations were solved in a segregated manner with the SIMPLE (Semi Implicit Pressure Linked Equation) algorithm. The second-order upwind scheme has been used for discretization. The under-relaxation parameters were set to 0.3 for pressure, 1 for density and body forces and 0.7 for momentum equations. All the solutions were considered to be fully converged when the sum of residuals was below 10^{-5}. All the computations have been performed on an HP, Z800 Work station with a Intel (R) Xeon (R) CPU with total of 24 GB RAM.

Table 5
Energy balance.

Case no.	Sr. no.	Velocity (ms^{-1})	Turbulent energy dissipation rate (W)		Mesh size
			CFD simulation	Experimental	
1	1	0.376	0.2426	0.2532	10,47,360 hexahedra
	2	0.482	0.5903	0.6212	10,47,360 hexahedra
	4	0.755	1.1466	1.3190	351,360 hexahedra
	4	0.755	1.2496	1.3190	10,47,360 hexahedra

4. Results and discussion

4.1. Energy balance

The Bernoulli equation is basically a mechanical energy balance. For incompressible flow, corrected for friction and kinetic-energy correction factors, it is given by

$$\frac{p_a}{\rho}+z_a+\frac{\alpha_a u_a^2}{2}=\frac{p_b}{\rho}+z_b+\frac{\alpha_b u_b^2}{2}+h_f \tag{8}$$

where each term represents mechanical energy effect based on unit mass of flowing fluid. In the modeling, the effect of friction (skin friction and form friction) has been taken into account by selecting standard k–ε model with wall function. Energy balance has been performed in all the cases by integrating the turbulent energy dissipation rate (ε) over entire volume and compared with power requirement:

$$Q\Delta p=\rho\int_V \varepsilon dV \tag{9}$$

Table 5 shows the overall energy balance. An excellent agreement (within 5 per cent) can be seen between the experimental and the predicted rates of turbulent energy dissipation.

4.2. Flow pattern

Velocity contour plot and velocity vectors are given in Fig. 4A and B, respectively. Fig. 5 shows the velocity profile upstream of orifice at z=0.15 m with a value of 0.85 for N (u_{avg}/u_{max}), which indicates the fully developed turbulent flow upstream of orifice meter. Similarly, fully developed velocity profile at z=0.4 m justifies the consideration of adequate length of the pipe downstream of orifice meter for the recovery of pressure. Narrowing of

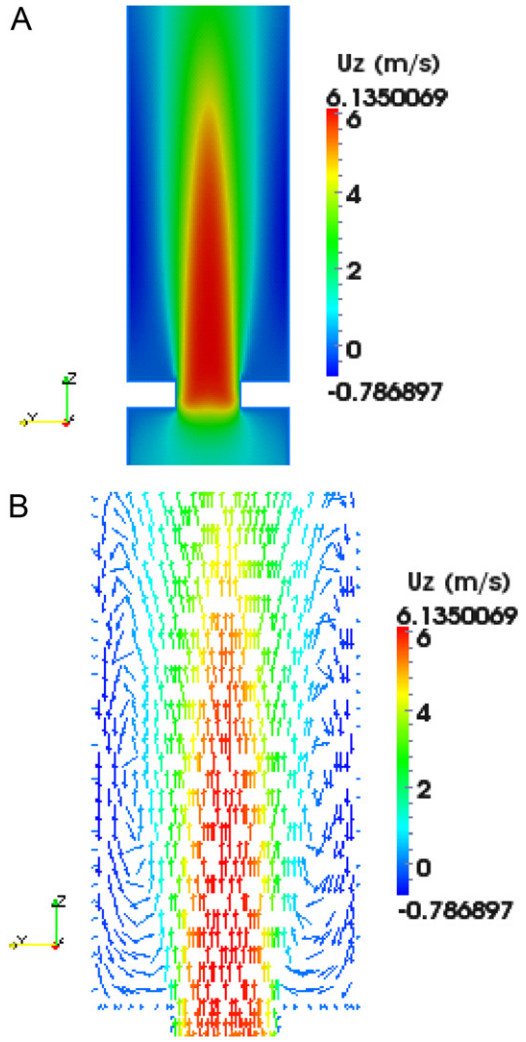

Fig. 4. (A) Velocity contours and (B) velocity vectors.

orifice jet shows the separation of boundary layer on the downstream side of orifice plate and forms a free flowing jet in the downstream fluid. Turbulent wakes and recirculation zones can be observed just downstream of orifice meter. In short, all the flow features expected for orifice flow have been observed in the numerical simulations.

4.3. Velocity and pressure profiles

Centerline axial velocity profiles for water and air are given in Figs. 2, 6 and 7. Centerline axial velocity increases as the flow approaches orifice meter. It further increases downstream of orifice meter and reaches at maxima. This point of maximum velocity is called vena-contracta. Beyond this point the velocity decreases. Energy has to be conserved at all the points in the domain, accordingly the pressure decreases when the flow approaches orifice meter, reaching minimum at vena-contracta and starts recovering as the flow moves further downstream. Excellent agreement can be seen between the predicted axial velocity profiles and the experimental measurements of Nail (1991) and Morrison et al. (1993) Similarly, excellent agreement can also be seen between the predicted wall pressure and experimental measurements of Nail (Re=18,400) and Morrison et al. (Re=91,100) with hexahedral mesh of 112,700 and 283,700, respectively. However, there is a faster recovery of pressure with downstream distance in case of simulation with higher Reynolds

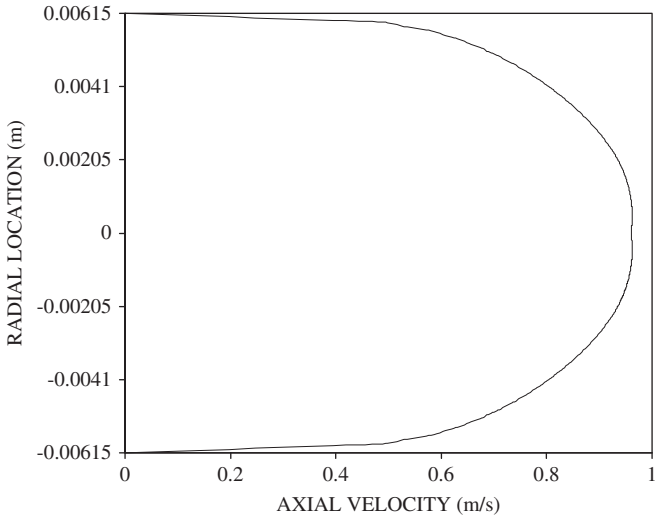

Fig. 5. Radial profile of axial velocity (for water) upstream of orifice at axial distance of z=0.15 m from entrance.

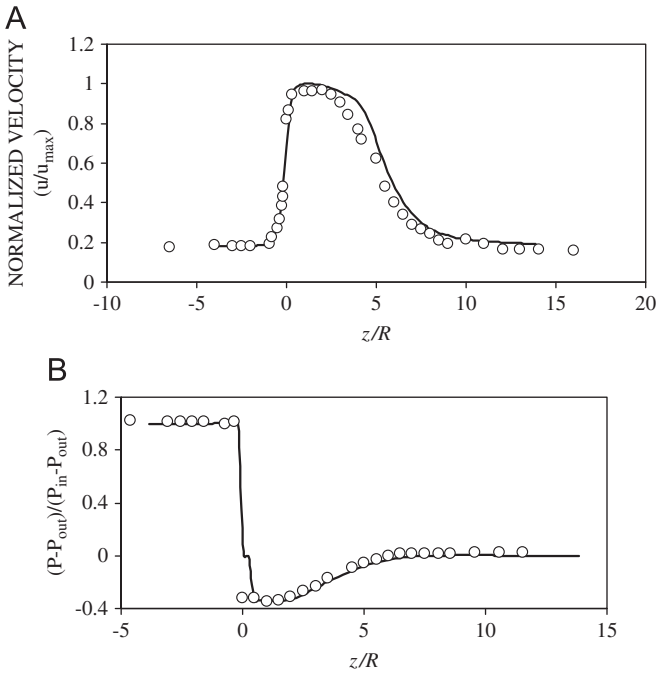

Fig. 6. Dimensionless (A) centerline axial velocity and (B) wall pressure profiles for air (Re=18,400), CFD simulations (—), Experimental data of Nail (O).

number (Re=91,100). This can be attributed to compressible nature of the air since the Mach no. (Ma) is of the order of 0.35 in the region near to orifice. This observation warns the readers to check the effect of compressibility on the pressure recovery profile downstream of orifice plate whenever the Mach no. is approaching 0.3 in near orifice region.

Radial profiles of axial velocity at various axial locations upstream and downstream of orifice plate are given in Fig. 8A and B. The gradual development of fully developed turbulent flow downstream of orifice meter from jet like profile is shown in Fig. 8B. It takes practically about z/R of 8.4 distances to reach to fully developed turbulent velocity profile. Variation in fraction of orifice differential with β is shown in Fig. 9. The plot indicates the reduction in pressure loss with an increase in the value of β. An excellent agreement can be seen between the CFD predictions and the values given by McCabe et al., 1993.

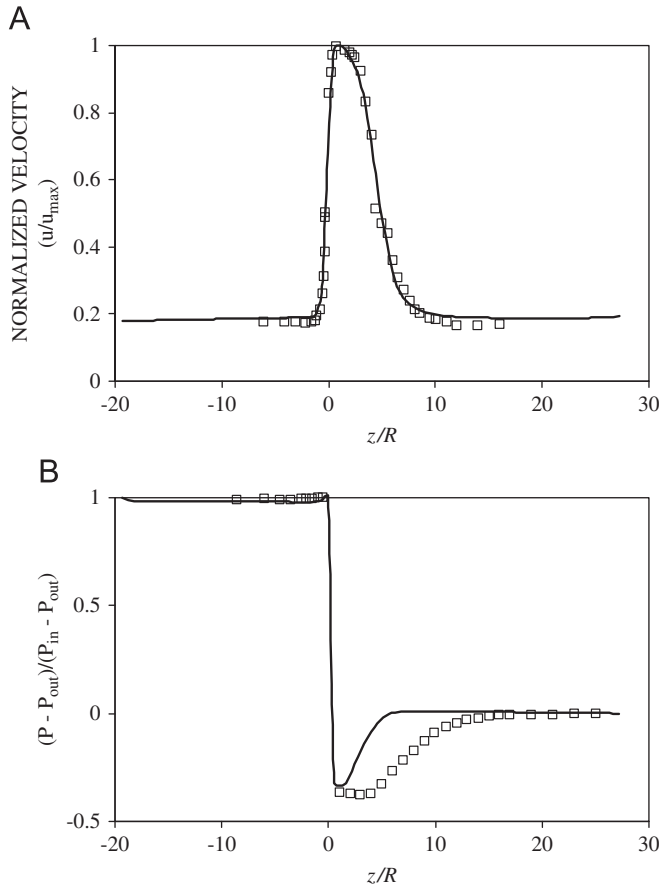

Fig. 7. Dimensionless (A) centerline axial velocity and (B) wall pressure profiles for air (Re=91,100), CFD simulations (—), Experimental data of Morrison (□).

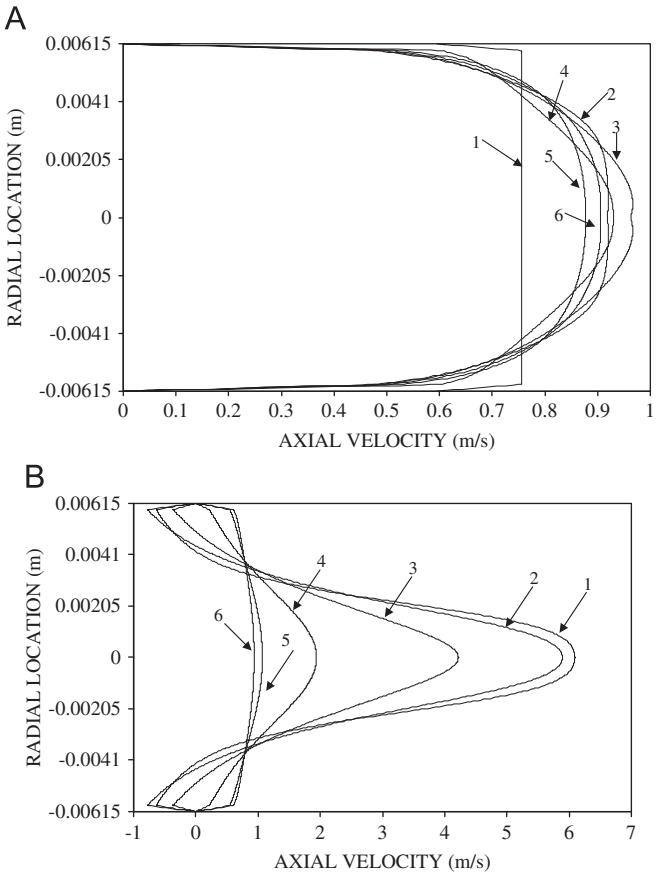

Fig. 8. Radial profiles of axial velocity at various axial locations. (1) z=0, (2) z=0.1, (3) z=0.2, (4) z=0.3, (5) z=0.4, (6) z=0.45. (A) Radial profiles of axial velocity at various axial locations close to downstream of orifice meter. (1) z=0.25, (2) z=0.26, (3) z=0.27, (4) z=0.28, (5) z=0.29, (6) z=0.30.

4.4. k and ε—profiles

Radial profiles of turbulent kinetic energy (k) and turbulent dissipation rate (ε) at various axial locations are shown in Figs. 10 and 11, respectively. Both have higher values near to wall in the fully developed upstream and downstream turbulent region because of higher velocity gradients. In the region, just after the orifice, highest velocity gradients are expected at the orifice jet wall, which forms due to the flow separation. Radial profile of mean axial velocity gradient just after the orifice is shown in Fig. 12, which shows that maximum velocity gradient is in the orifice jet boundary, which is expected to form at a diameter lesser than orifice diameter (5 mm). The profile of velocity gradient also indicates the flow separation. Turbulent kinetic energy (k) and turbulent energy dissipation rate (ε) are also at maximum at the jet wall region as shown in Figs. 10B and 11B, respectively. Both figures show the gradual development of k and ε profiles from orifice plate to fully developed turbulent flow in the downstream of orifice meter.

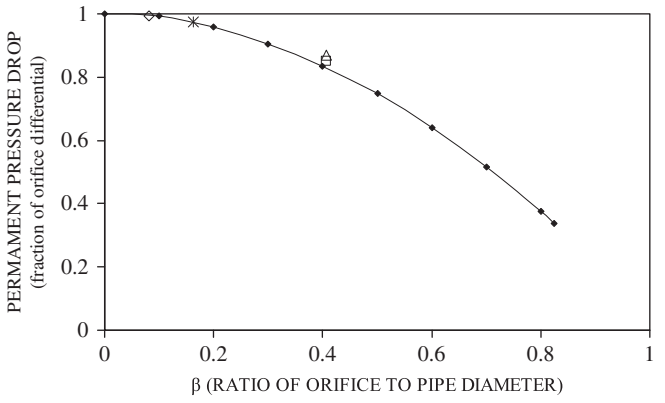

Fig. 9. Variation in orifice loss coefficient with β. McCabe and Smith (—◇—), β=0.4065 (□, coarse grid), β=0.4065 (△, fine grid), β=0.162 (⊗), β=0.0813 (O).

4.5. Discharge coefficient (C_D) and pressure drop–velocity relationship

Table 6 gives the experimental and simulated values of discharge coefficient. Experimental measurements of Δp has been taken to calculate experimental values of C_D whereas from CFD, C_D has been calculated with Δp predicted by CFD between upstream of orifice and vena-contracta at which the wall pressure is minimum. Following equation has been used to obtain C_D:

$$C_D = \frac{u_0\sqrt{(1-\beta^4}}{\sqrt{\Delta p/\rho}} \tag{10}$$

Further, CFD predictions of flow rate versus square root of pressure drop for flange taps and vena-contracta taps is given in Fig. 13. The relation comes out to be linear for vena-contracta tap in the water flow velocity upto 3 ms^{-1}, which is permissible

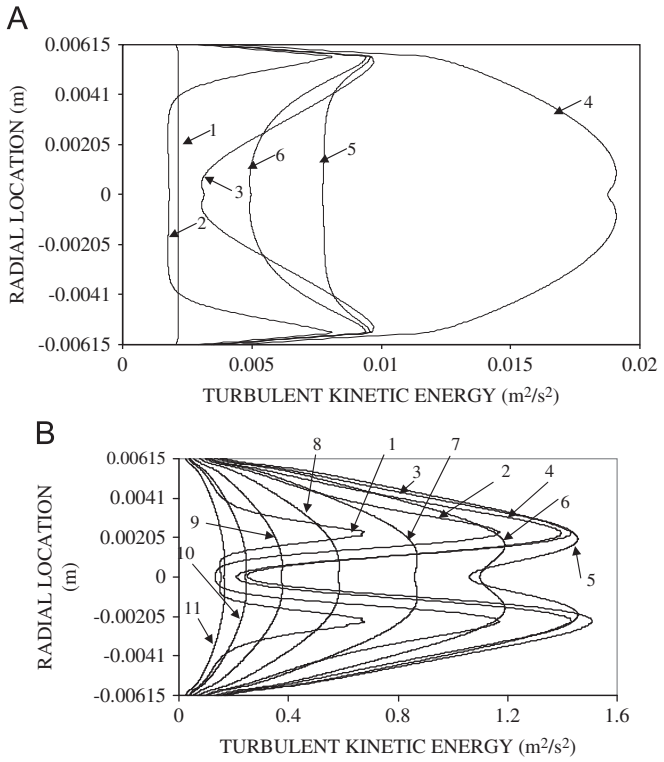

Fig. 10. Radial profiles of turbulent kinetic energy (k) at various axial locations. (1) $z=0$, (2) $z=0.05$, (3) $z=0.2$, (4) $z=0.35$, (5) $z=0.4$, (6) $z=0.45$. (B) Radial profiles of turbulent kinetic energy (k) at various axial locations close to downstream of orifice meter. (1) $z=0.25$, (2) $z=0.255$, (3) $z=0.26$, (4) $z=0.265$, (5) $z=0.27$, (6) $z=0.275$, (7) $z=0.28$, (8) $z=0.285$, (9) $z=0.29$, (10) $z=0.295$, (11) $z=0.3$.

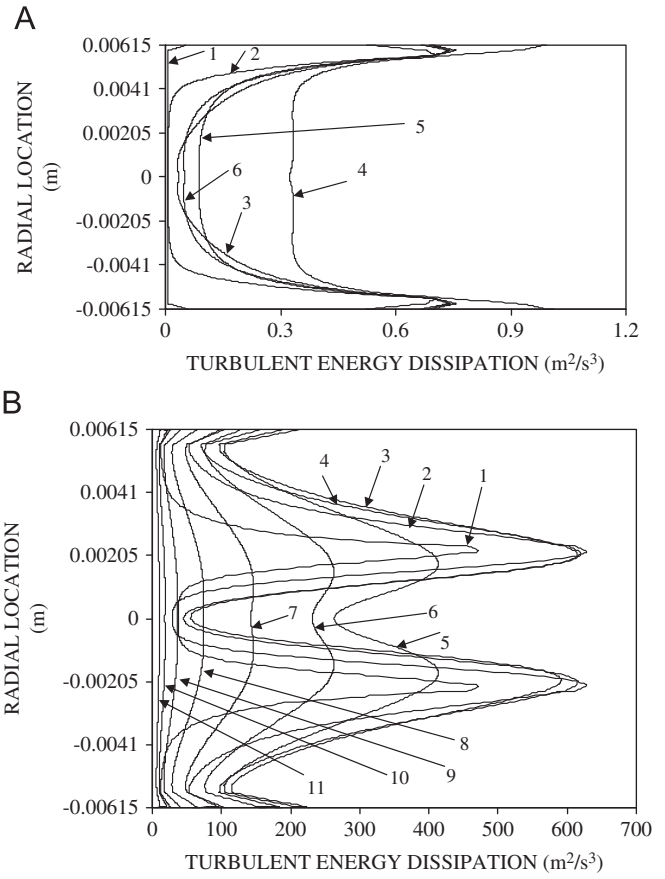

Fig. 11. (A) Radial profiles of turbulent dissipation rate (ε) at various axial locations. (1) $z=0$, (2) $z=0.05$, (3) $z=0.2$, (4) $z=0.35$, (5) $z=0.4$, (6) $z=0.45$. (B) Radial profiles of turbulent dissipation rate (ε) at various axial locations close to downstream of orifice meter. (1) $z=0.25$, (2) $z=0.255$, (3) $z=0.26$, (4) $z=0.265$, (5) $z=0.27$, (6) $z=0.275$, (7) $z=0.28$, (8) $z=0.285$, (9) $z=0.29$, (10) $z=0.295$, (11) $z=0.3$.

velocity of liquid in pipe. Apart from this linear relationship, vena-contracta taps measure maximum pressure drop and hence can give flow measurement with more sensitivity.

4.6. Sensitivity analysis of k–ε turbulence model parameters (C_μ, σ_k, σ_ε)

Effects of change in k–ε turbulence model parameters on radial profiles of turbulent kinetic energy (k) and turbulent dissipation rate (ε) at an axial location of $z=0.28$ m from inlet are shown in Figs. 14–16. Table 7 shows the effects of variation in C_μ (0.05, 0.09, 0.14), σ_k (1.0, 1.4, 1.8) and σ_ε (1.0, 1.3, 1.6) on energy balance and C_D. Change in the profiles of k and ε have been observed for variation in the value of C_μ (Fig. 14) and σ_ε (Fig. 16) at a location downstream of orifice plate. No appreciable change has been observed in the profiles for variation in σ_k (Fig. 15). However, not much variation has been observed in the value of integral of ε and hence in discharge coefficent (Table 7). Changes in profiles of k and ε, due to variation in C_μ and σ_ε, change the pressure profile downstream of orifice leading to small variation in discharge coefficients as reported in Table 7. Simulations have also been performed to study the sensitivity of turbulent intensity (3%, 5% and 7%) for specifying the boundary conditions for k and ε. Fig. 17 shows the effect of variation in turbulent intensities on k and ε profile. No appreciable changes have been observed. Similar analysis pertaining to other geometries is available in the published literature by Ranade and co-workers (Ranade et al., (1989, 1991, 1992); Ranade and Joshi (1990)) for pitched bladed turbine, disk turbine, agitated tanks and axial flow impellers. Patwardhan and Joshi (1999), Sahu et al. (1998, 1999) and Sahu and Joshi (1995) have also reported similar sensitivity analysis for stirred vessels.

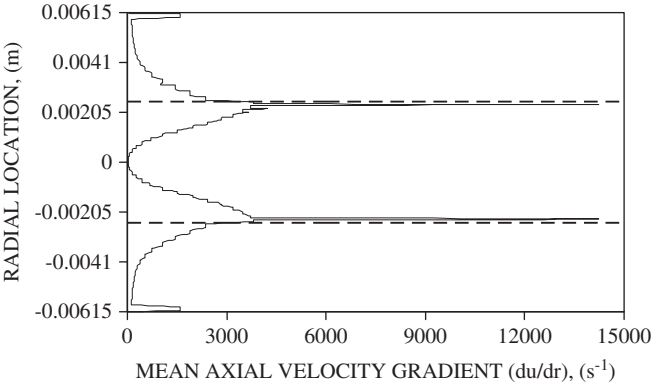

Fig. 12. Mean axial velocity gradient just after the orifice at z=0.25. CFD simulation (—), Orifice diameter (———).

4.7. A conceptual new design for locating vena-contracta

It is known that the location of vena-contracta depends upon Re and β. Therefore, it was thought desirable to propose a conceptual scheme to physically locate the vena-contracta in an orifice meter (in Fig. 18). It has two parts in addition to conventional orifice meter. First part is the flexible below,

Table 6
Details of experiments conducted with water as fluid and the values of orifice coefficient.

Sr. no.	Q (ml/s)	ΔP (N/m^2)	Inlet velocity (ms^{-1})	Velocity at throat (ms^{-1})	Pipe *Re*	Discharge coefficient	
	(measured)	(measured with flanged taps)	(calculated)	(calculated)	(calculated)	Experimental	CFD simulation
1	44.67	5680.08	0.376	2.275	4489	0.6657	0.6253
2	57.33	10,866.24	0.482	2.920	5762	0.6177	0.6128
3	80	23,461.20	0.673	4.074	8040	0.5866	0.6035
4	89.67	29,511.72	0.755	4.567	9012	0.5863	0.5996

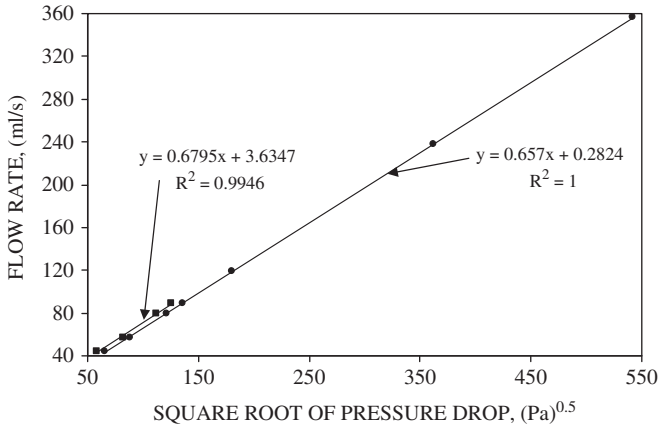

Fig. 13. Variation in flow rate with square root of pressure drop across orifice meter. Experiment with flange taps (■), CFD prediction with vena-contracta taps (●).

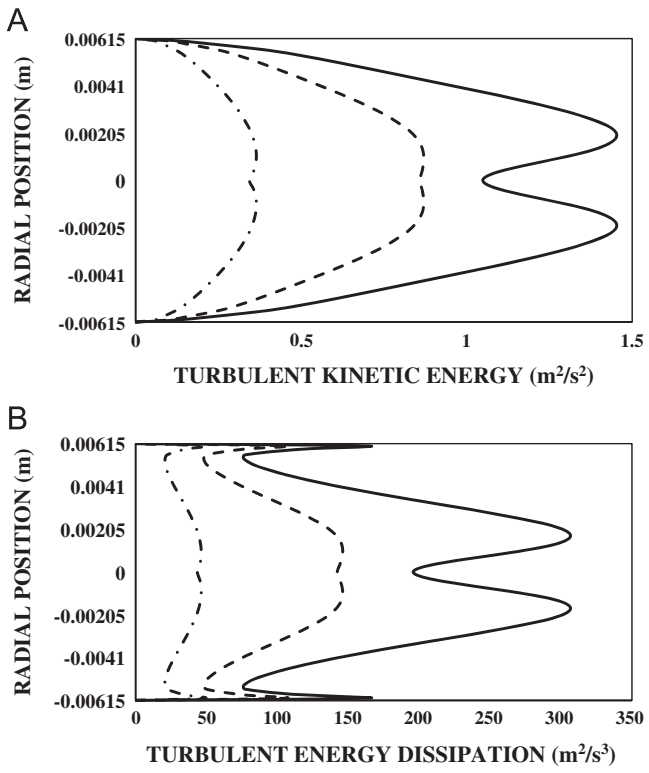

Fig. 14. Effect of Cμ on (A) *k* profile and (B) ε profile at z=0.28 m; C_μ=0.05 (—), C_μ=0.09 (– – –), C_μ=0.14 (– · – ·).

which allows axial movement of vena-contracta tap within the slot made on pipe at the downstream of orifice meter. Second part is the mounting tie rods to position vena-contracta tap at a location. The proposed scheme allows replacement of an orifice

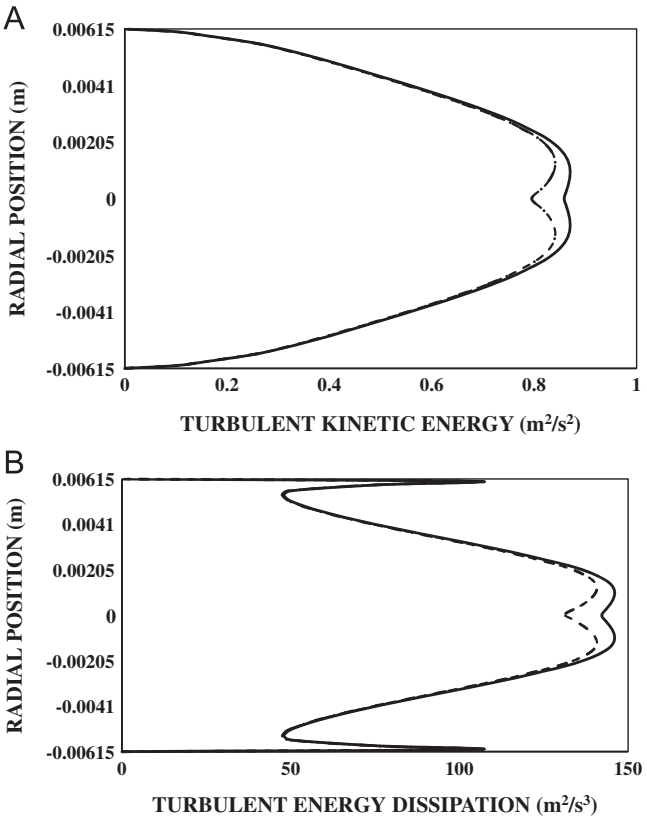

Fig. 15. Effect of σ_k on (A) *k* profile and (B) ε profile at z=0.28 m; σ_k=1.00 (—), σ_k=1.40 (– – –), σ_k=1.80 (– · – ·).

plate for different range of flow rates and permits the positioning also of vena-contracta without affecting the seals by loosening and tightening the nuts, fixed on mounting tie rods. A slot provided in pipe surface just after the orifice, not only guides the vena-contracta pressure tap but also restricts its movement within design parameters. Separate bolt holes are provided for mounting orifice plate to avoid leakage through flange.

The location of vena-contracta can be estimated from CFD simulations. It is the location of minimum wall pressure near the downstream of orifice. There is a provision in the proposed scheme of orifice hardware to physically locate the pressure tap downstream of orifice plate at vena contracta. Also, it is possible to design the proposed scheme for a given orifice meter for a given process conditions and tested before it is put into actual application. Alternatively, the vena-contrcta location can be identified through hardware (by relatively positioning the two parts) so as to get maximum pressure drop. It can be noted that the new design does not hamper the existing advantages of orifice meter and offers measurement with better accuracy and sensitivity.

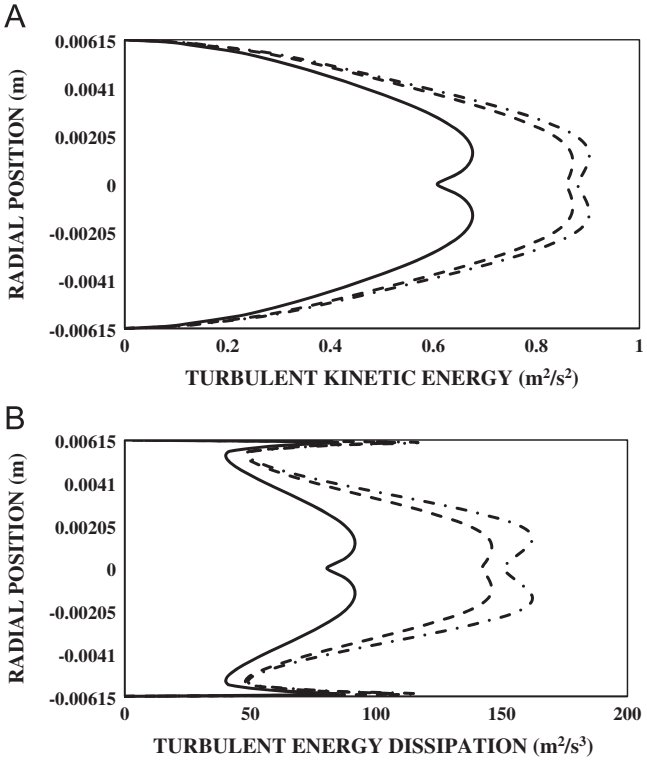

Fig. 16. Effect of σ_ε on (A) k profile and (B) ε profile at z=0.28 m; σ_ε=1.00 (—), σ_ε=1.30 (– – – –), σ_ε=1.60 (– · – ·).

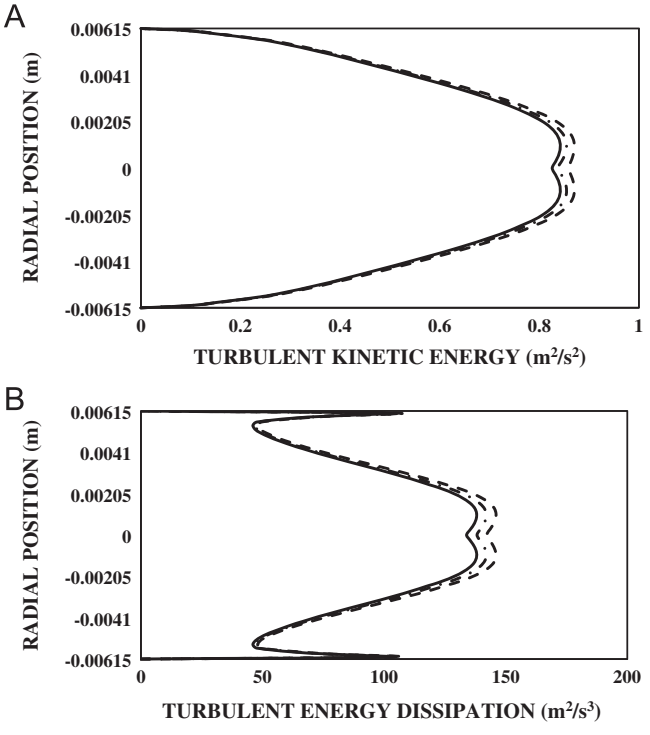

Fig. 17. Effect of turbulent intensity on (A) k profile and (B) ε profile at z=0.28 m; Turbulent intensity of 3% (—), 5% (– – – –), 7% (– · – ·).

Table 7
Sensitivity of k–ε turbulence model parameters on turbulent energy dissipation rate and discharge coefficient.

Sr. no.	C_μ	σ_k	σ_ε	Turbulent intensity (%)	$\int_V \varepsilon dV \times 10^{-3}$ (m^5/s^3)	C_D
1	0.09	1	1.3	5	1.2496	0.5996
2	0.05	1	1.3	5	1.1647	0.6052
3	0.14	1	1.3	5	1.2783	0.5975
4	0.09	1.4	1.3	5	1.1385	0.6158
5	0.09	1.8	1.3	5	1.1385	0.6158
6	0.09	1	1	5	0.9322	0.6279
7	0.09	1	1.6	5	1.2369	0.5998
8	0.09	1	1.3	3	1.2337	0.6017
9	0.09	1	1.3	7	1.2543	0.5983

5. Conclusions

Flow through an orifice meter has been simulated, successfully, using CFD technique using OpenFOAM-1.6 solver. Very good agreement between experimental data and CFD predictions viz. energy balance, flow pattern, pressure recovery, velocity profiles, pressure profiles and sensitivity analysis of turbulence model parameters, validates the CFD predictions and also the applicability of standard k–ε turbulence model for capturing turbulence effect in orifice flow. It is also concluded that the CFD technique can be used as an alternative and cost effective tool towards replacement of experiments required for estimating discharge coefficient, empirically. Validity of proposed design of an orifice meter with a provision to track vena-contracta using CFD technique has been explained with the predicted linear relationship between flow rate and maximum pressure drop through an orifice($Q \propto \sqrt{\Delta P}$), however, its performance has to be evaluated, experimentally, in small size pipeline before using the design for higher bore pipelines.

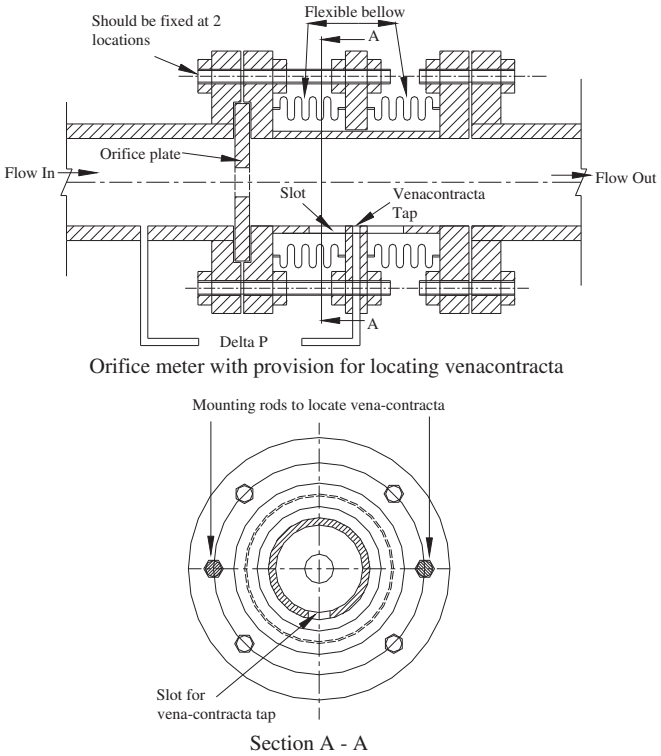

Fig. 18. Conceptual scheme of tracking the vena-contracta.

Notation

C_D	Discharge coefficient (dimensionless)
D	pipe diameter (m)
d	orifice diameter (m)
P	pressure drop (N m^{-2})
G_k	generation of turbulence kinetic energy due to the mean velocity gradients (kg m^{-1}s^3)
I_T	turbulent intensity (%)
k	turbulent kinetic energy per unit mass (m^2 s^{-2})
L	length of pipe (m)
L_U	length of pipe before orifice plate in an orifice meter (m)
L_T	total length of an orifice meter (m)
Ma	Mach number (u/u_{sonic}) (dimensionless)
N	ratio of average velocity to the maximum velocity (u_{avg}/u_{max}) in a pipe
Q	volumetric flow rate (m^3 s^{-1})
Re	Reynolds number ($\rho ud/\mu$) (dimensionless)
$\lvert\bar{S}\rvert$	mean strain rate (s^{-1})
$\bar{S}_{ij}$	strain rate (s^{-1})
t	orifice plate thickness (m)
u_i	velocity component (ms^{-1})
$\langle u \rangle$	time averaged of velocity (ms^{-1})
Y	any distance along the diameter of pipe (m)
y^+	dimensionless distance from the wall (dimensionless)
z	any distance along the length of pipe from inlet (m)

Greek symbols

β	ratio of orifice diameter to pipe diameter (dimensionless)
Δ	difference in a quantity
ε	turbulent energy dissipation rate per unit mass (m^2 s^{-3})
μ	kinematics viscosity (m^2 s^{-1})
μ_{eff}	*effective* viscosity of fluid (Pa s)
ν_t	turbulent viscosity (m^2 s^{-1})
ρ	density of fluid (kg m^{-3})
σ_k	turbulent Prandtl number for kinetic energy
σ_ε	turbulent Prandtl number for energy dissipation rate
τ_ϖ	shear stress at the wall (N m^{-2})

Subscript

avg	*average*
eff	effective
in	inlet
k	kinetic energy as in *k*
max	maximum
out	outlet
Upstream	upstream of orifice in a pipe
Total	total in pipe length

Abbreviation

CFD	Computational Fluid Dynamics

Acknowledgment

This work has been a part of the project supported by the Department of Atomic Energy (DAE), Government of India.

References

Durst, F., Wang, A.B., 1989. Experimental and numerical investigation of the axisymmetric, turbulent pipe flow over a wall-mounted thin obstacle. In: Seventh Symposium on Turbulent Shear Flows, Stanford University, pp. 21–23.
Erdal, A., Andersson, H.I., 1997. Numerical aspects of flow computation through orifices. Flow Meas. Instrum. 8, 27–37.
Ho, Y.S., Leung, T.P., 1985. Performance of conical entrance orifice plates at low Reynolds numbers. Intern. J. Heat Mass Transfer 6, 122–125.
Husain, Z.D., 2010. Theoretical uncertainty of orifice flow measurement. Daniel Measurement and Control White Papers, 〈www.daniel.com〉.
Launder, B.E., Spalding, D.B., 1972. Mathematical Models of Turbulence. Academic Press, London.
McCabe, W.L., Smith, J.C., Harriott, P., 1993. Unit operations of Chemical Engineering, Fifth edition McGraw-Hill International Editions, Singapore.
Morrison, G.L., DeOtte Jr., R.E., Nail, G.H., Panak, D.L., 1993. Mean velocity and turbulence fields inside a β=0.50 orifice flowmeter. AIChE J. 39, 745–756.
Nail, G.H., 1991. A study of 3-Dimensional flow through orifice meters, Ph.D. Dissertation, Texas A&M University, USA.
Naveenji, A., Malavarayan, S., Kaushik, M., Sriananth, H., 2010. CFD analysis on discharge coefficient during non-Newtonian flows through orifice meter. Int. J. Eng. Sci. Technol. 2, 3151–3164.
Oliveira, N.M.B., Vieira, L.G.M., Damasceno, J.J.R., 2010. Numerical methodology for orifice meter calibration. Mater. Sci. Forum 660, 531–536.
Patwardhan, A.W., Joshi, J.B., 1999. Relation between flow pattern and blending in stirred tanks. Ind. Eng. Chem. Res. 38, 3131–3143.
Ranade, V.V., Bourne, J.R., Joshi, J.B., 1991. Fluid mechanics and blending in agitated tanks. Chem. Eng. Sci. 46, 1883–1893.
Ranade, V.V., Joshi, J.B., 1990. flow generated by a disc turbine ii: mathematical model. T. I. Chem. Eng (UK)—A: Chem. Eng. Res. Des. 68, 34–50.
Ranade, V.V., Joshi, J.B., Marathe, A.G., 1989. Flow generated by pitched bladed turbine Part II: Mathematical modelling and comparison with experimental data. Chem. Eng. Commun. 81, 225–248.
Ranade, V.V., Mishra, V.P., Saraph, V.S., Deshpande, G.B., Joshi, J.B., 1992. Comparison of axial flow impellers using LDA. Ind. Eng. Chem. Res. 31, 2370–2379.
Sahu, A.K., Joshi, J.B., 1995. Simulation of flow in stirred vessels with axial flow impellers: effects of various numerical schemes and turbulent model parameters. Ind. Eng. Chem. Res. 34, 626–639.
Sahu, A.K., Kumar, P., Joshi, J.B., 1998. Simulation of flow in stirred vessel with axial flow impeller: zonal modelling and optimization of parameters. Ind. Eng. Chem. Res. 34, 626–639.
Sahu, A.K., Kumar, P., Patwardhan, A.W., Joshi, J.B., 1999. CFD modelling and mixing in stirred tanks. Chem. Eng. Sci. 54, 2285–2293.
Smith, E., Ridluan, A., Somravysin, P., Promvonge, P., 2008. Numerical investigation of turbulent flow through a circular orfice. KMITL Sci. 8, 43–50.
Thakre, S.S., Joshi, J.B., 2000. CFD modelling of heat transfer in turbulent pipe flow. AIChE J. 54, 5055–5060.
Thakre, S.S., Joshi, J.B., 2002. Momentum, mass and heat transfer in single phase turbulent flow. Rev. Chem. Eng. 18, 83–293.
Vander Vorst, H.A., 1981. Iterative solution methods for certain non-symmetric matrix arising from pde-problems. J. Comput. Phys. 44, 1–19.
Versteeg, H.K., Malalasekera, W., 1995. An introduction to computational fluid dynamics: The finite volume method. Pearson Education Limited, England.